Enhanced Photocatalytic and Filtration Properties of Carbon-Doped g-C_3N_4 Membranes Reinforced with Nanofibrillated Cellulose

Beiyue Xiong,[a,#] Yirong Liu,[a,#] Wenbiao Zheng,[a,b] Xiaoxiao He,[a] Chengning Ye,[a,c] Hanyu Xue ,[a,*] Jianrong Xia ,[a] Renjin Gao,[a] and Liwei Wang [a,*]

*#: These authors contributed equally; *Corresponding author: 366157115@qq.com (H.X.); wlw@mju.edu.cn (L.W.)*

DOI: 10.15376/biores.20.1.809-825

GRAPHICAL ABSTRACT

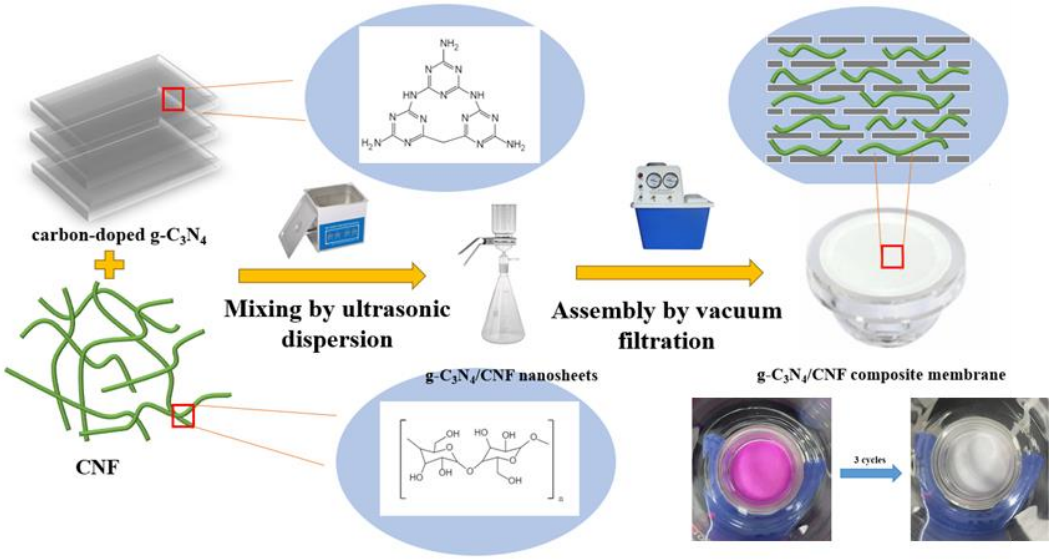

Enhanced Photocatalytic and Filtration Properties of Carbon-Doped g-C_3N_4 Membranes Reinforced with Nanofibrillated Cellulose

Beiyue Xiong,[a,#] Yirong Liu,[a,#] Wenbiao Zheng,[a,b] Xiaoxiao He,[a] Chengning Ye,[a,c] Hanyu Xue ,[a,*] Jianrong Xia ,[a] Renjin Gao,[a] and Liwei Wang [a,*]

Carbon-doped g-C_3N_4 was synthesized using a simple high-temperature process (calcination at 550 °C for 4 h). One-dimensional nanofibrillated cellulose (NFC) materials were then inserted into the two-dimensional g-C_3N_4 material by vacuum filtration method at room temperature. The prepared g-C_3N_4/NFC composite membranes were systematically characterized using a series of techniques, such as XRD, FTIR, and SEM. The results showed that the carbon-doped photocatalysts possessed a narrow band gap, which prolonged the visible light absorption and favored the organic pollutant degradation. The incorporation of NFC enlarged the interlayer spacing, leading to an increase in the water flux. The water flux of $C_{0.02}$CN/NFC (15%) composite membranes reached 73.7 L•m^{-2}•h^{-1}•bar^{-1}, which is more than that of g-C_3N_4/NFC membrane. At the same time, the carbon doped composite membranes showed enhanced retention and photocatalytic degradation ability. The retention rate of the $C_{0.02}$CN/NFC (5%) composite membranes could reach 89.3% from 80.8% after three-cycle photocatalytic experiments. The membrane maintained a good retention rate and feed flux, which confirms the composite membrane has good self-cleaning ability and stability. It could potentially be applied for water treatment.

DOI: 10.15376/biores.20.1.809-825

Keywords: Graphitic phase carbon nitride; Photocatalysis; Composite membrane; Cellulose; Water flux

Contact information: a: College of Materials and Chemical Engineering, Minjiang University, Fuzhou 350108, China; b: College of Environment and Safety Engineering, Fuzhou University, Fuzhou 350116, China; c: College of Materials Engineering, Fujian Agriculture and Forestry University, Fuzhou 350002; #: These authors contributed equally;
** Corresponding author: 366157115@qq.com (H.X.); wlw@mju.edu.cn (L.W.)*

INTRODUCTION

Industrialization produces large quantities of polluted water streams that adversely affect the entire ecosystem and are therefore a serious problem for the global environment. If large quantities of organic dye wastewater and antibiotic wastewater are discharged directly into natural water bodies without treatment, it will result in serious environmental pollution and waste of resources, threatening human life, health, and safety (Fouda *et al.* 2021; Liang *et al.* 2021; Asaithambi *et al.* 2022). Therefore, there is a great desire to develop green and sustainable technologies to address the water pollution problems associated with global industrialization.

Conversion of solar energy into sustainable fuels and chemicals using semiconductor-type photocatalysts has become a widely used technology in sustainable and environmentally clean development (Hussain *et al*. 2021; Dou *et al*. 2022; Hussain *et al*. 2022). Various semiconductors, such as sulfides, oxides, and nitrides, have been

investigated as active photocatalysts for many years (Hou *et al*. 2021; Zhang *et al*. 2021; Rehman *et al*. 2022). However, the photocatalysts are usually nanoscale powders, and nanoscale powders are not ideal for practical purposes, especially for water treatment, because they are difficult to remove from water after photocatalytic treatment. Thus, the catalysts are difficult to recover and reuse. Photocatalytic nanoparticles remaining in the water are also prone to cause health hazards to humans or animals. To overcome these shortcomings, the combination of membrane filtration and photocatalysis has been proposed, *i.e.*, the use of a photocatalytic layer to modify the membrane function.

The photocatalyst is initially exposed to light in a photocatalytic process, which results in the production of photoexcited e and h^+ in the valence band (VB) and conduction band (CB), respectively. The excited e^+ and h^+ then break apart, causing the photocatalytic reaction to start on the semiconductor surface. Ultimately, the combination and reaction of the electrons (reductive agent) and holes (oxidative agent) with adsorbed electron acceptors and donors, respectively, determines the synthesis of the necessary products in the photocatalytic reaction. The efficiency of nanomaterials needs to be increased to satisfy engineering goals, especially in solar photocatalysis (Chakravorty and Roy 2024). In recent years, the nonmetallic semiconductor photocatalyst g-C_3N_4 has been widely used in the fields of pollutant degradation, water purification, and CO_2 because of the advantages of its simple process, good chemical stability, suitable bandgap (Kuang *et al.* 2024; Liu *et al*. 2020; Yang *et al*. 2023; Wang *et al*. 2024; Wen *et al.* 2017), and the ability to produce hydrogen. However, the narrow visible light adsorption range and high photogenerated electron-hole recombination rate of g-C_3N_4 lead to its low photocatalytic efficiency. Many techniques have been used to improve the photocatalytic efficiency of g-C_3N_4, including changing the morphological structure (Wang *et al*. 2021), doping with heteroatoms (Jiang *et al*. 2017), and coupling with different semiconductors (Wang *et al*. 2022). Among these modification methods, doping of non-metallic elements can enhance the photocatalytic activity of g-C_3N_4 without causing secondary pollution to the environment, which has a good application prospect (Mohammad *et al*. 2020). Carbon is one of the most common non-metallic elements in nature, with non-toxic and harmless properties, and is commonly used in the manufacture of semiconductors. Therefore, carbon doping may bring benefits to the photocatalytic performance of g-C_3N_4, and carbon self-doping has non-toxic and harmless properties.

Cellulose and its derivatives, as biocompatible polymers, have attracted considerable attention for various applications due to suitable physical and mechanical properties. Cellulose naturally develops functionality, flexibility, and high specific strength by exploiting hierarchical structure and also has low density, low price, as well as biodegradability (Seddiqi *et al.* 2021). Nano-fibrillated cellulose is a cellulose material that is at the nanometer level size in at least one-dimensional direction, with a diameter of generally 1.0 nm to 100 nm. NFC is hydrophilic and can be used in a manner similar to a surfactant to promote the dispersion of carbon nanotubes (CNTs) and graphene-like carbon materials (Huang *et al*. 2022; Zhou *et al.* 2023). The oxygen-containing groups on the surface of NFC also contribute to the formation of a good affinity for polar polymers, and NFC can serve as a matrix skeleton. The NFC can be used as a matrix skeleton, dispersant, and adhesive to prepare high-performance flexible composites. Composite films prepared with cellulose have excellent properties such as good ductility (Samuel *et al*. 2020). In addition, the hydroxyl groups in NFC can promote the adsorption of organic pollutants and accelerate the efficiency of photogenerated electron transfer, thus significantly improving the photodegradation efficiency of composites (Seddiqi *et al.* 2021).

In this study, the structure of g-C_3N_4 was firstly regulated by citric acid as a dopant with urea calcined at high temperature, and then g-C_3N_4 composite membranes were fabricated by layer-by-layer self-assembly assisted by vacuum filtration using undoped/ doped g-C_3N_4 and commercial nanocellulose (NFC) (Wu *et al*. 2022). The hybridization of the NFCs in the undoped/doped g-C_3N_4 can effectively regulate the nanochannel sizes and improve the stability and flexibility. The presence of NFC resulted in an increase in the water flux. The membrane maintained a good retention rate and feed flux, which confirms the composite membrane has good self-cleaning ability and stability.

EXPERIMENTAL

Materials

Urea (Sinopharm Chemical Reagent Co., Ltd., Shanghai, China), anhydrous ethanol (Xilong Science Co. Ltd., Chengdu, China), nanofibrillated cellulose (Fig.1, Qihong Science and Technology Co., Ltd., Guilin, China), rhodamine B and citric acid (Fuchen Chemical Reagent Factory, Tianjin, China), PTFE film with pore size 0.22 μm and diameter 47 mm (Chuangwei Filtration Equipment Factory, Haining, China) were used in this study. All the chemicals are analytical grade without further treatment.

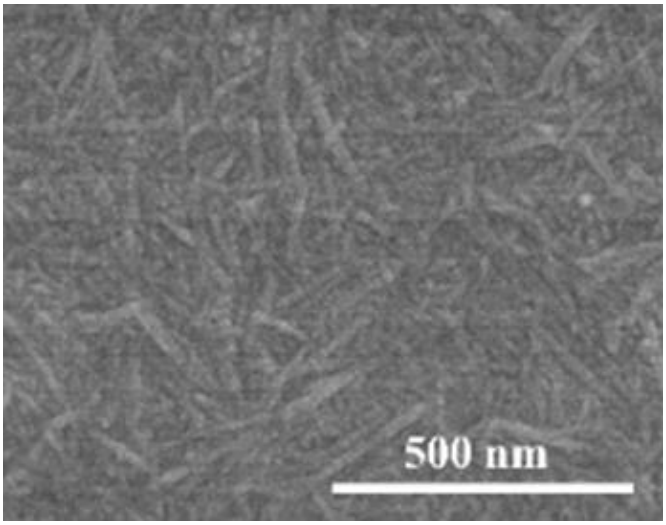

Fig. 1. SEM image of nanofibrillated cellulose

Preparation of Carbon-Doped g-C_3N_4 (CCN)

Twenty grams of urea and a certain amount of citric acid were dissolved in 25 mL of deionized water, and then the solution was placed in an oven at 60 ℃ to maintain a constant temperature for 24 h to obtain a white powdery product. This was then loaded into a sealed ceramic crucible for calcination at 550 ℃ for 4 h, with a heating rate of 2.2 ℃/min, to obtain a yellow powder, *i.e.*, a carbon-doped g-C_3N_4, as shown in Schematic 1a. The same method was used to synthesize carbon-doped g-C_3N_4 samples of different carbon masses, respectively. Citric acid amounts of 0.005, 0.01, and 0.02 g were used to prepare different carbon-doped g-C_3N_4 samples, named C$_X$CN (X indicates the mass of citric acid).

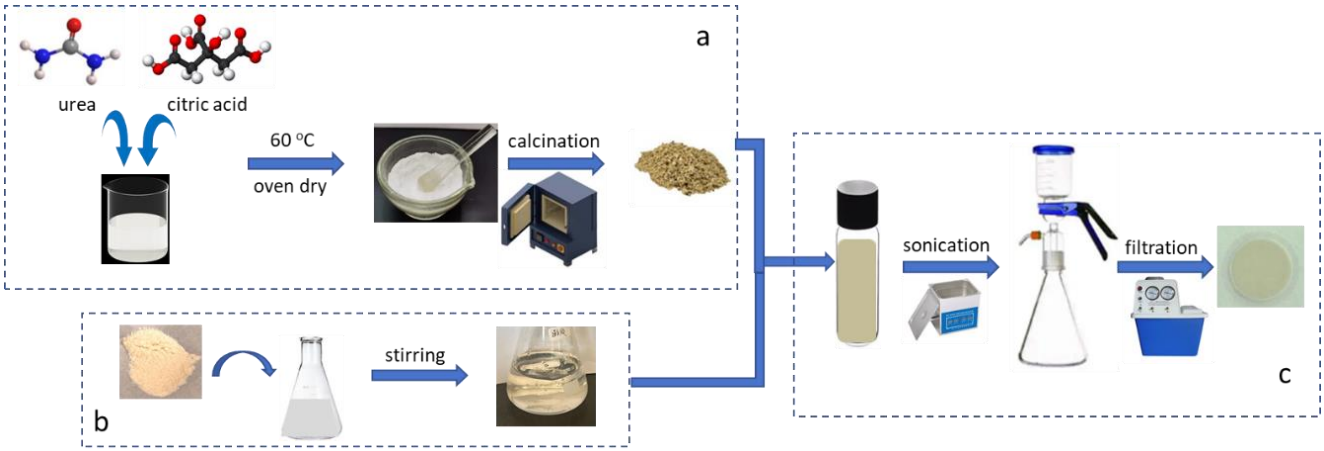

Scheme 1. Schematic illustration of (a) synthesis of CCN, (b) preparation of NFC gel and (c) fabrication of the composite membrane

Preparation of Cellulose Nanofiber (NFC) Gel

1 g of nanofibrillated cellulose and 99 g of water were mixed at room temperature by vigorous stirring until a homogeneous and transparent gel was obtained (Schematic 1b).

Preparation of Carbon-Doped g-C_3N_4/NFC (CCN/NFC) Composite Membranes

Approximately 15 mg of carbon-doped g-C_3N_4 was mixed with different ratios (5%, 10%, 15%) of NFC, and 30 mL of 30% ethanol was then added, to form a carbon-doped g-C_3N_4/NFC suspension. When no obvious carbon-doped g-C_3N_4 particles were observed on the surface of the solution, the suspension was ultrasonicated for about 8 h. Then, it was filtered using a PTFE microporous membrane under vacuum, and the product obtained from filtration was air-dried at room temperature for about 24 h to obtain the carbon-doped g-C_3N_4/NFC (CCN/NFC) composite membrane (Schematic 1c).

Characterization

XRD test: X-ray diffraction (XRD) patterns of the g-C_3N_4 and CCN were collected using a diffractometer (Rigaku, Japan) in reflection mode from 10° to 35° (2θ) in steps of 0.02° (40 kV, 100 mA) with Cu Kα radiation ($\lambda = 1.5419$ Å, 40 kV, 40 mA).

SEM test: An SU8010 scanning electron microscope (SEM) (Hitachi, Japan) was used to observe the microscopic morphology of the samples. The membranes to be tested were glued to a sample stage with conductive adhesive as required, then sprayed with gold, and the images were captured with a 20 kV incident electron beam.

UV-Vis test: Ultraviolet-visible (UV-Vis) spectroscopy was determined by a UV-2600 spectrometer (Shimadzu, Japan).

FTIR test: Fourier transform infrared (FTIR) spectroscopy was performed within the range of 500 to 4000 cm^{-1} using a NICOLET IS50 FTIR spectrometer (Thermo fisher, USA).

EDS test: Energy dispersive X-ray spectroscopy (EDS) of samples were obtained by a Nano GmBH TM X-ray spectrometer (Bruker, Germany).

XPS test: The chemical compositions of the specimen and surface element content were characterized by ESCALAB 250X X-ray photoelectron spectrometer (XPS, VG Corporation, USA).

Membrane Performance Evaluation

Water flux

The water flux test was performed on a dead-end filtration device at room temperature. The composite g-C_3N_4 or CCN/NFC nanofiltration membranes were placed in a filter cup with an effective test radius of 1.5 cm. After controlling the nitrogen pressure to 1.0 bar and compacting with distilled water for 10 min to ensure the membrane was fully wet and no air between the membrane and base, the distilled water flux V (L) through the membrane at time *t* is measured. Then, the pure water flux J_0 of the g-C_3N_4 or CCN/NFC composite membrane was obtained using Eq. 1,

$$J_0 = \frac{V}{A\mathrm{t}} \quad (1)$$

where J_0 is the water flux through the membrane (L/(m²•h)), *t* is the time (h), *V* is the volume of liquid through the membrane at time *t* (L), and *A* is the effective area of the membrane (m²).

Retention and self-cleaning properties

The retention performance of the composite membranes was evaluated by measuring the absorbance of the solution under UV light before and after the transmission of Rhodamine B dye through the membrane. The measured dye rejection, R, was calculated as in Eq. 2,

$$R = (1 - \frac{A}{A_0}) \times 100\% \quad (2)$$

where *A* and A_0 are the absorbances of the transmembrane dye and the absorbance of the original dye, respectively (Abs). The self-cleaning performance of the membranes was evaluated by measuring the flux recovery before and after photocatalytic treatment of the composite membrane surface. A 10 mg/L solution of rhodamine B was prepared and tested for four consecutive times under nitrogen pressure for the retention and flux through the carbon nitride nanosheet membrane at time *t*. The flux J_a for the first time, the flux J_b for the second time, the flux J_c for the third time, and the flux J_d for the fourth time. The integrated photocatalytic-filtration experiments were carried out using a 300 W xenon lamp as a photocatalytic light source simulating the sunlight illumination for 1 h. The dye pollutants were removed from the composite membranes while the fluxes and retention of the composite membranes were tested again at 15 min intervals and recorded every 15 min as J_e, J_f, J_g, and J_h. The flux recovery (F_R) of the composite membrane was deduced by applying the calculation method of Eq. 3 and compared to explore the self-cleaning performance of the membrane,

$$F_{RR} = \frac{J_h}{J_a} \times 100\% \quad (3)$$

where J_h is the flux after membrane photocatalysis in units of (L•m^{-2}•h^{-1}•bar^{-1}); J_a is the first flux before membrane contamination in units of (L•m^{-2}•h^{-1}•bar^{-1}).

Photocatalytic properties

A composite was put into a photoreactor with 200 mL of 10 mg/L Rhodamine B solution. The solution was kept stirring under dark conditions for 1 h to ensure that the adsorption and desorption processes reached an equilibrium state. Then, a 350 W xenon

lamp was turned on to catalyze the solution. During the process, 3 mL of solution sample was collected every 20 min using a syringe. The absorbance of the supernatant being sonicated was measured at a wavelength of 553 nm. The degradation efficiency is calculated using Eq. 2.

RESULTS AND DISCUSSION

Characterization of Carbon-Doped g-C_3N_4 samples

Various CCN samples prepared from different contents of carbon-doped g-C_3N_4 were subjected to XRD tests, and the resulting spectra are shown in Fig. 2a. Two distinct peaks were observed from the XRD pattern in all the samples; one was a higher intensity diffraction peak of (002), which matches with the interplanar aromatic systems stacking peak (Shibu *et al.* 2024), while a low intensity diffraction peak of (100) is compatible with the inter-layer structure of the lattice planes. These peaks are in agreement with the previous studies (Zhu *et al*. 2019; Praus 2022). The CCN sample still has the characteristic peaks of g-C_3N_4, which indicates that the incorporation of carbon-doped material did not change the crystal structure of g-C_3N_4 and did not produce other crystal structures. Meanwhile, compared with g-C_3N_4, the values of the 2θ of peak (002) of doped samples were slightly shifted towards the higher values of 2θ, which indicates that the carbon doping reduces the stacking spacing of the g-C_3N_4 monolayers according to the Bragg equation.

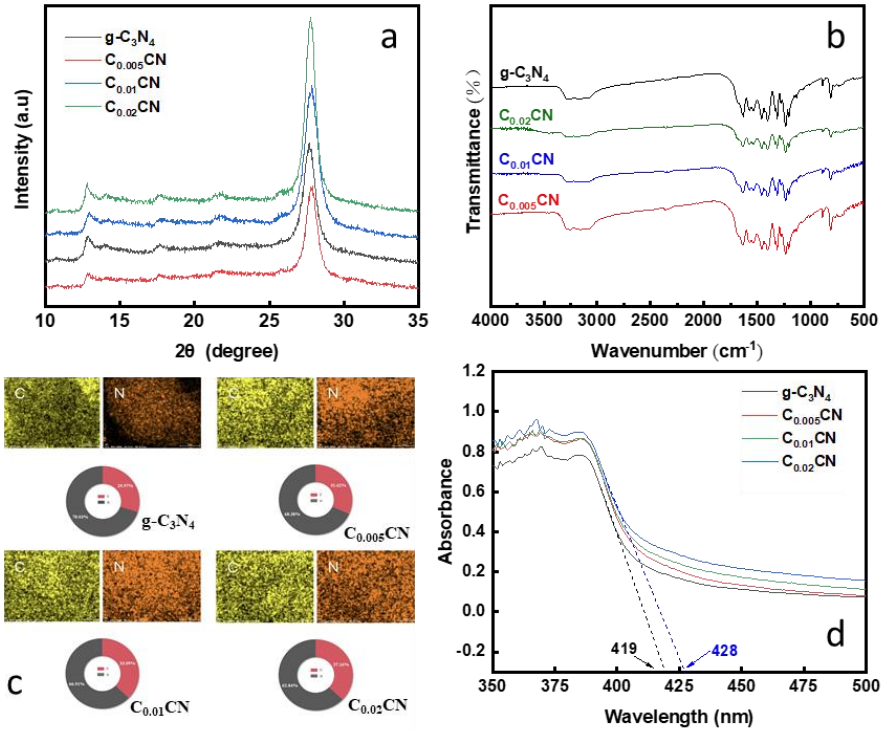

Fig. 2. (a) XRD patterns, (b) FTIR patterns, (c) EDS plots and (d) UV-Vis diffuse reflectance spectra of g-C_3N_4, $C_{0.005}$CN, $C_{0.01}$CN, and $C_{0.02}$CN

Further, the carbon content increased, and the intensity of the characteristic peaks of the (002) crystal surface was higher than that of g-C_3N_4, indicating that the carbon-doped

g-C_3N_4 material affected the ordered structure of g-C_3N_4 with a higher degree of crystallinity. No noticeable shift of the peaks to lower values was observed in the (100) crystal face, which indicates that the flat face inter-aperture distances of tris-s-triazine did not change noticeably. Furthermore, all the samples exhibited the characteristic infrared images of g-C_3N_4 without noticeable change (Fig. 2b), indicating that the main skeleton of g-C_3N_4 has not been destroyed during the doping process.

For further understanding of the chemical composition, the samples were checked with energy dispersive spectra (EDS) of elemental mapping energy dispersive X-ray (EDX) mode. Figure 2c shows the EDS plots of the composite films with different carbon doping amounts, from which it can be seen that the total mass occupied by C atoms gradually increases with the increase of the carbon doping content, in which the mass of C atoms of $C_{0.02}CN$ increases from 30.0% (g-C_3N_4) to 37.2% ($C_{0.02}CN$), which indicates that the carbon atoms have been successfully introduced into the g-C_3N_4. Figure 2c also shows the uniform distribution of elements of nitrogen and carbon. No other impurity elements are present in the synthesized materials (Shibu *et al.* 2024).

Ultraviolet diffuse reflectance spectroscopy (UV-Vis DRS) was used to investigate the optical absorption properties and band gap of the carbon-doped samples and g-C_3N_4. As shown in Fig. 2d, compared with g-C_3N_4, $C_{0.02}CN$ were red-shifted to a certain extent on the optical absorption edge, and the light absorption was stronger, in which the absorption edge of g-C_3N_4 was near 419 nm, while $C_{0.02}CN$ photo-absorption out edge was near 428 nm, which indicates that CCN can utilize more energy of the visible light band. Using the Tauc model and the UV–Vis spectra as a basis, the band gap energy (E_g) of the samples was calculated (Shibu *et al.* 2024), and the results are listed in Table 1. With the addition of doped carbon, the bandgap width of g-C_3N_4 decreased from 2.86 to 2.76 eV ($C_{0.02}CN$). The doped samples exhibited a narrower bandgap, which helps significantly reduce the recombination process of photogenerated charge carriers, thereby effectively enhancing the catalytic ability of the photocatalysis (Sahoo *et al.* 2022).

Table 1. Band Gap of Undoped/doped C_3N_4 Samples

Samples	g-C_3N_4	$C_{0.005}CN$	$C_{0.01}CN$	$C_{0.02}CN$
Band gap (eV)	2.86	2.83	2.79	2.76

The XPS spectra of g-C_3N_4 and $C_{0.02}CN$ were compared to analyze the effect of carbon doping on the chemical bonds on the chemical properties of the specimen. As displayed in Fig. 3a and 3b, no significant changes in the C 1s and N 1s spectra were observed, indicating similar chemical states of C and N elements in the catalyst samples. These findings showed that the doping of carbon had little effect on the structure of the triazine ring, which is consistent with FTIR analysis. As shown in Fig. 3a, the characteristic peak at 284.8 eV in g-C_3N_4 corresponds to C-C in the triazine ring, and 288.2 eV corresponds to sp^2 hybridized carbon (N-C=N) (Hafeez *et al.* 2020). The N 1s XPS spectra can be deconvoluted into three peaks with binding energies of 398.8, 400.3, and 404.4 eV, corresponding to the sp2-hybridized N atoms, the sp3-hybridized N atoms, and charging effects on the triazine ring N, respectively (Zhou *et al.* 2019). In addition, the C/N atomic ratio of $C_{0.02}CN$ increased from 0.034 (g-C_3N_4) to 0.072 ($C_{0.02}CN$), which is similar to the observation of EDS. Those results indicate that carbon atoms were introduced into g-C_3N_4, meaning that doping with citric acid introduced additional carbon atoms, likely due to the replacement of N atoms by C.

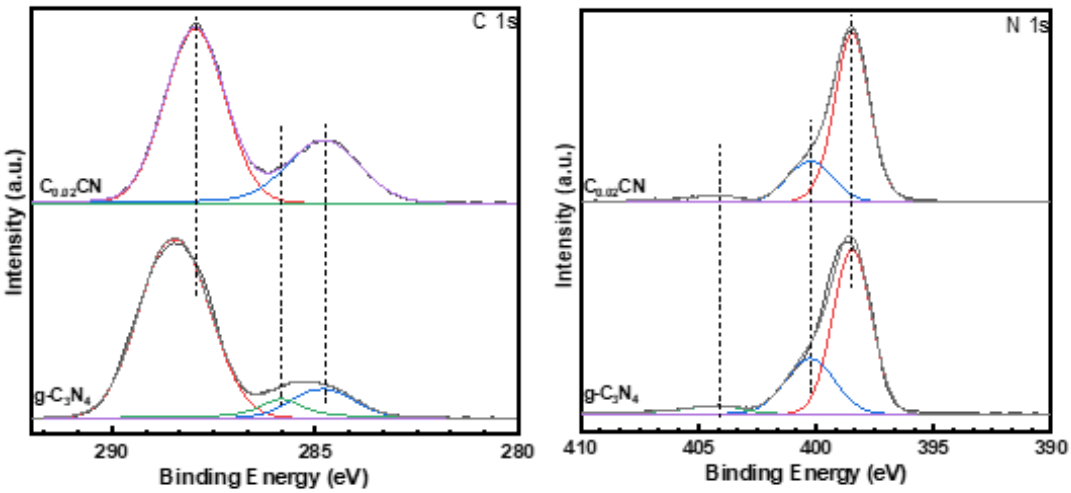

Fig. 3. (a) C 1s and (b) N 1s XPS spectra of g-C_3N_4 and $C_{0.02}CN$

Characterization of Composite Films

To investigate whether NFC was successfully inserted into the g-C_3N_4 lamellae, the surface and cross-section of composite membranes with different ratios of the same carbon-doping content were characterized. It can be seen from Fig. 4(a to c) that, through vacuum filtration, g-C_3N_4 layer were stacked layer-by-layer on the surface of the PTFE-based membrane to form a clear and distinct g-C_3N_4/NFC, which is similar to other reported works (Zhou *et al.* 2023; Pan *et al.* 2023).

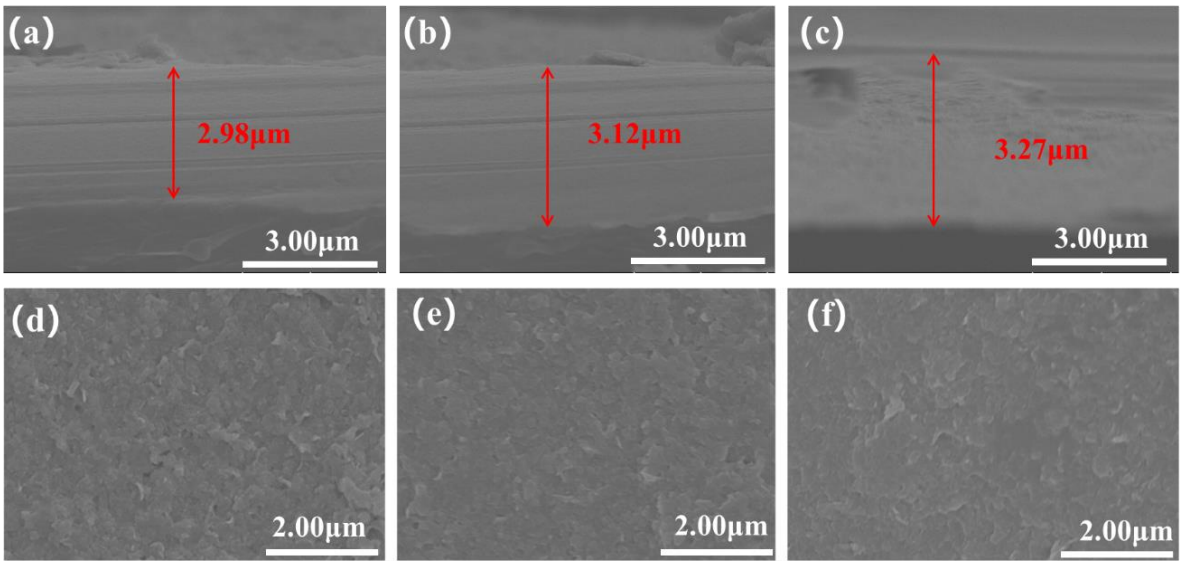

Fig. 4. SEM images of composite membranes with different NFC ratios: Cross-sections of (a) 5%, (b) 10%, (c) 15% NFC composite membrane; and surface views of (d) 5%, (e) 10%, and (f) 15% NFC composite film

Meanwhile, membrane gradually became thicker with the increase of NFC content (5%, 10%, 15%), which initially confirms the effective intercalation of NFC molecules between the membranes (Zhou *et al.* 2023). Furthermore, the channels generated from the stacking of NFC can act as molecular sieves, allowing the water to pass through while rejecting solutes, which is similar to the pores in conventional polymeric membranes (Shen *et al.* 2021).

The top view morphologies of the membrane with different carbon doping were obtained to study the membrane surface microstructures. It was observed that a smooth and dense layer was successfully formed on the surface of the PTFE substrate due to the layer-by-layer assembly of the layered g-C_3N_4 sheets. The g-C_3N_4/NFC layer played the role of separating small molecules. During filtration, water molecules and some small molecules passed through the interlayer of the functional layer, while substances with sizes larger than the interlayer spacing were retained (Zhou *et al.* 2023).

Water Flux Tests

The water flux of various CCN/NFC composite membranes was investigated by adjusting the layer spacings of g-C_3N_4 nanosheets using NFC. Figure 5 shows the water flux tests of composite membranes prepared by doping different carbon contents and mass ratios of NFC. The proportion of NFC is a key factor for membrane modification. When the ratio of NFC was lower than 5%, it is difficult to fabricate the uniform membrane. However, when the ratio of NFC was higher than 20%, the durability of the membrane decreased. Therefore, the ratio of NFC was chosen at the range of 5 to 15%.

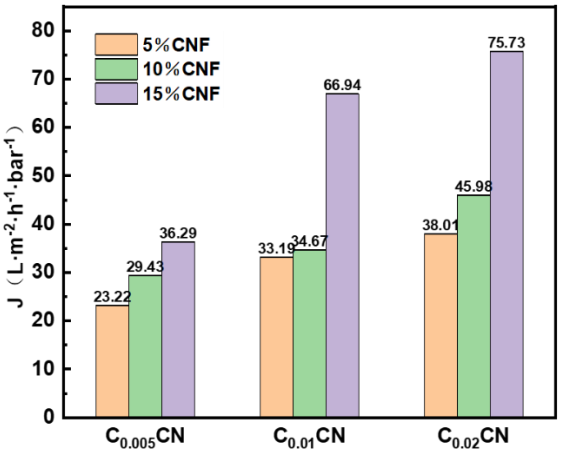

Fig. 5. Effect of carbon doping amount and NFC contents on water flux of the membrane

For $C_{0.02}CN$ composite membrane, the pure water flux increased from 38.0 to 75.7 $L•m^{-2}•h^{-1}•bar^{-1}$ when the NFC content was increased from 5% to 15%. An increase in the proportion of NFC increased the water flux of the g-C_3N_4/NFC composite membrane, which is attributed to the fact that NFC, as a one-dimensional material, is inserted between the two-dimensional material of g-C_3N_4, which forms a stable and effective support between the layers through the interaction force. This makes the original narrow interlayer structure gradually open, providing an additional transmembrane transport pathway for water molecules (Zhou *et al.* 2023). The g-C_3N_4 interlayer spacing can be enlarged by increasing the proportion of NFC, thus increasing the water flux of the composite membrane. In addition, the water flux of the composite membranes tends to increase with

the increase of carbon doping. The water flux of $C_{0.02}CN$/NFC composite membrane reaches the maximum value of 73.7 $L•m^{-2}•h^{-1}•bar^{-1}$ when the proportion of NFC is at 15%.

Retention and Self-Cleaning Properties

Rhodamine B (RhB) was chosen as a representative dye because of its small molecular size, which makes it difficult to be removed by conventional filtration techniques. The risk of RhB carcinogenicity and neurotoxicity to humans and animals are well documented (Zhou *et al*. 2019). Because carbon doping and NFC content are crucial for photocatalytic membranes, the effects of carbon doping and NFC on the retention and self-cleaning properties of g-C_3N_4/NFC membranes were investigated. Figure 6 shows the effect of g-C_3N_4/NFC composite membranes with different carbon doping amounts and different NFC ratios on the feed flux and retention of the membrane. As shown in Fig. 6a, the flux of the membrane became bigger when more carbon was added. Similarly, the flux was also increased with increasing of NFC content. Those result is same to the water flux of the membrane observed in Fig. 5. Regarding the retention efficiency, it was observed from Fig. 6b that in the absence of carbon doping (*i.e.*, g-C_3N_4/NFC membranes), the retention percentage on the membranes was low (R = 49.0%). With the increase of carbon doping amount, the retention increased. The retention of $C_{0.02}CN$/NFC (5%) could reach 80.8%. This indicates that carbon doping could improve the retention rate of the membrane. However, the retention decreased gradually with increasing NFC ratio. This is attributed to the fact that the pore channel of the composite membrane became larger as the proportion of NFC increased (Zhou *et al*. 2023). Thus as the feed flux increased, the retention capacity decreased.

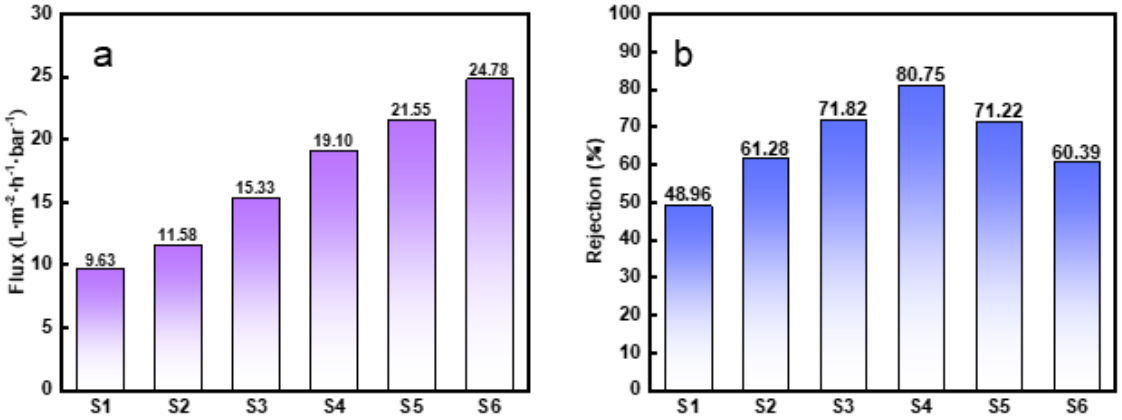

Fig. 6. Effect of carbon doping amount and NFC contents on and feed fluxes (a) and retention (b) of the membrane (S1: g-C_3N_4/NFC(5%); S2: $C_{0.005}CN$/NFC(5%); S3: $C_{0.01}CN$/NFC(5%); S4: $C_{0.02}CN$/NFC(5%); S5: $C_{0.02}CN$/NFC(10%); S6: $C_{0.02}CN$/NFC(15%))

To highlight the advantages of the prepared photocatalytic membranes, the integrated photocatalytic-filtration process was carried out under different irradiations, and the retention efficiency and feed flux of the composite membranes changed considerably by switching from dark to light irradiation conditions. Based on the consideration of flux and retention, the photocatalytic test was conducted on the membrane with 5% NFC. In Figs. 7a and b are the test results of the feed flux and retention rate of the same membrane recycled four times under the same conditions without light irradiation. It can be seen that the retention and flux were highest during the first cycle and then decreased with cycle

times. Furthermore, the membrane with high carbon content, the retention and feed flux dropped significantly, such as the retention and flux were decreased from 81% to 31% and from 19.10 to 8.41 $L \cdot h^{-1} \cdot m^{-2} \cdot bar^{-1}$, respectively. Overall, the feed flux and retention performance of the membrane decreased after several cycles of retention, which may be due to the clogging and swelling caused by the enrichment of dye molecules into the water channel (Yang *et al.* 2023).

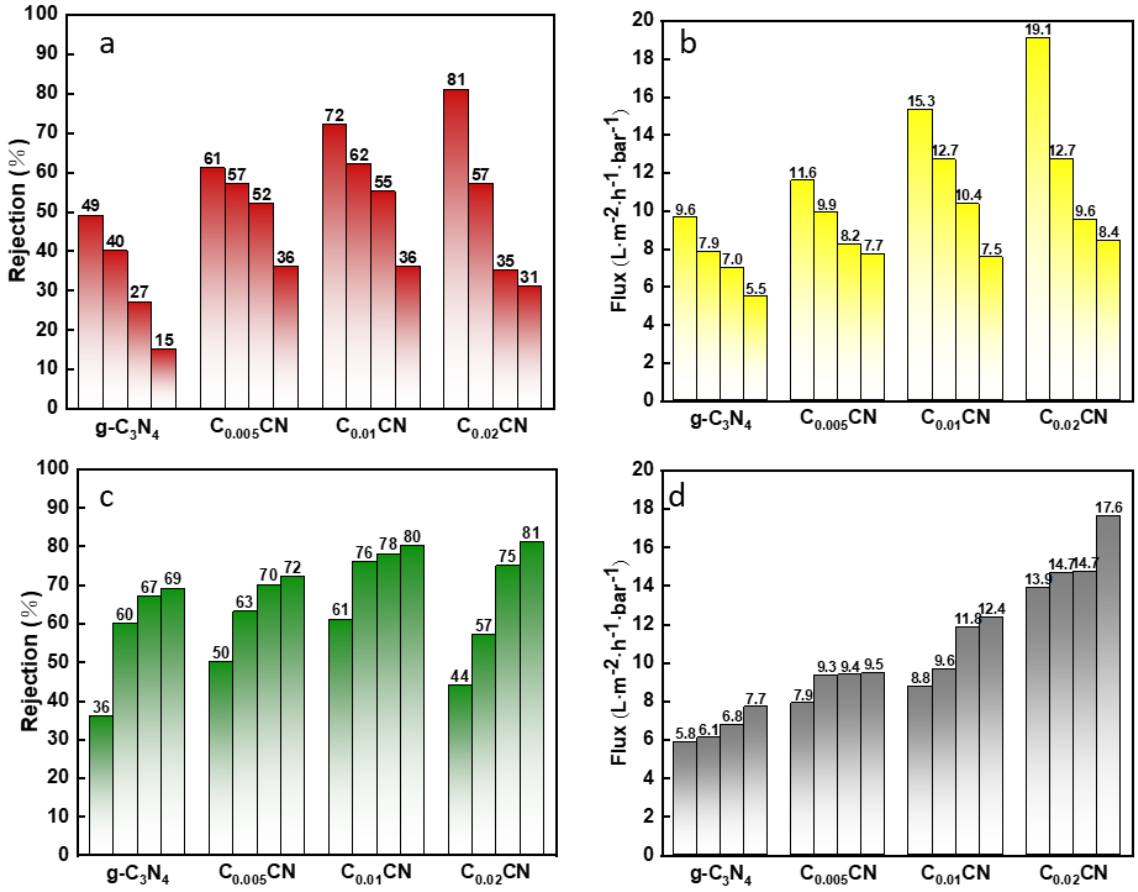

Fig. 7. Retention rate and feed flux of composite membranes before and after light exposure with different carbon doping content and 5% NFC content: (a) Retention rate of composite membrane before illumination; (b) Feed flux of composite membrane before illumination; (c) Retention rate of composite membrane after illumination; and (d) Feed flux of composite membrane after illumination

Figures 7c and d show the results of the feed flux and retention tests on g-C_3N_4/NFC composite membranes under the light irradiation condition. When xenon lamp was on, the flux and retention of the composite membranes recovered gradually with the increase of the number of retention cycles. After four cycles, the retention and flux of $C_{0.02}$CN/NFC membrane were increased to 81% and 17.63 $L \cdot h^{-1} \cdot m^{-2} \cdot bar^{-1}$, respectively. This confirmed the critical role of photocatalysts under light irradiation. Furthermore, the retention efficiencies of the composite membranes were higher than that of original membrane except for $C_{0.02}$CN/NFC. This is probably because the higher content of carbon doping in the composite membranes resulted in a higher degradation rate (Cao *et al.* 2018).

To confirm speculation proposed above, the photocatalytic activity of the membrane with different carbon doping amount was evaluated. As shown in Fig. 8, the

composite membrane without carbon doping performed relatively poorly in catalytic degradation, only 28.7% of degradation rate could be reached after 6 h. With the increase in carbon doping, the degradation rate of the composite membrane on RhB also gradually increased. The photocatalytic ability was the highest when the carbon doping amount was 0.02 g, with a degradation effect of 40.5% achieved at 6 hours. Therefore, this fully demonstrates that carbon doping indeed enhanced the catalytic activity of the composite membrane.

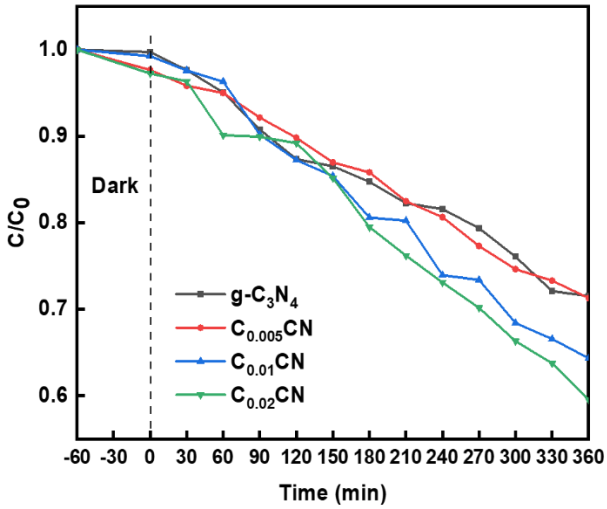

Fig. 8. Photocatalytic ability of composite membranes with different carbon doping

To further explore the self-cleaning performance of these membranes, the authors calculated and analyzed flux recovery percentages ($F_{R)}$ as shown in Table 2. A higher F_R indicates a more effective self-cleaning performance. The flux recovery after photocatalytic irradiation of the $C_{0.02}$CN/NFC (5%) composite membrane reached 92.3%, *i.e.*, the strongest self-cleaning performance. The experimental results demonstrated the key role of the composite membranes under light irradiation as well as the effective photocatalytic ability of the composite membranes.

Table 2. Flux Recovery Rates of Composite Membranes

Film Type	g-C_3N_4	$C_{0.005}$CN	$C_{0.01}$CN	$C_{0.02}$CN	$C_{0.02}$CN	$C_{0.02}$CN
NFC Ratio (%)	5	5	5	5	10	15
F_R (%)	80.0	81.6	80.7	92.3	83.2	82.4

Moreover, based on the above study, long-term stability tests (3 consecutive cycles, corresponding to about 6 h of total processing time) of the as-prepared $C_{0.02}$CN/NFC (5%) membrane were conducted for the integrated photocatalysis-filtration process for RhB treatment under xenon lamp irradiation (simulating sunlight). As shown in Fig. 9, the flux as well as the dye retention rate of the composite membrane with the number of times after cyclic testing on the surface of the composite membrane under light irradiation are plotted. As can be seen from the figure, the trends of the feed flux and the retention rate showed regular fluctuations during the three on/off cycles. Under light irradiation, the flux of the solution recovered to 16 to 18 $L•m^{-2}•h^{-1}•bar^{-1}$ with a retention of 80% to 90%. However, in the absence of light irradiation (*i.e.*, membrane function only), the flux and retention significantly decreased to 8 to 12 $L•m^{-2}•h^{-1}•bar^{-1}$ and 15% to 45%. In addition, the retention of the composite membrane was improved after three cycles. The experimental results

showed that the composite membranes maintained good retention and feed fluxes throughout the three cycle experiments, confirming the good self-cleaning ability and long-term stability of the composite membranes.

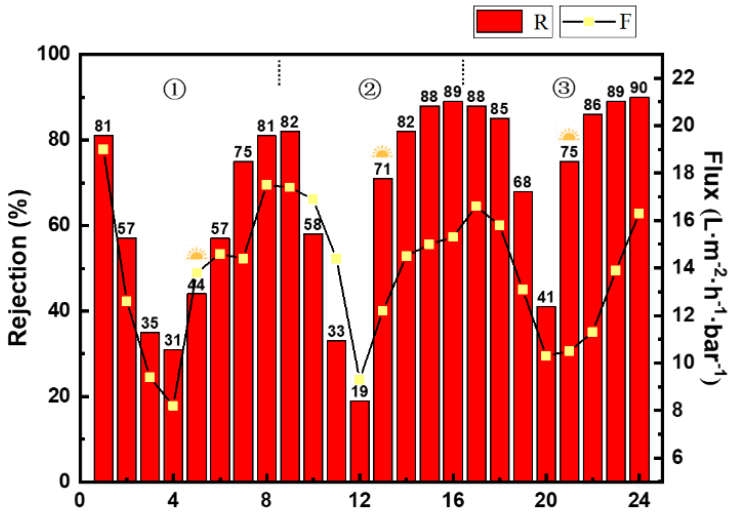

Fig. 9. Retention *versus* feed flux of $C_{0.02}$CN/NFC (5%) composite membranes tested with three cycles of self-cleaning

The membrane after three cycles of photocatalytic filtration application is shown in Fig. 10. The surface of the composite membrane was very clean and the color was almost restored to its original state, so that no additional cleaning treatment is required in practical applications. Through comparing the performance with and without irradiation conditions, it is obvious that the integrated photocatalytic process was superior to the simple filtration process in removing dyes (Pan *et al*. 2023).

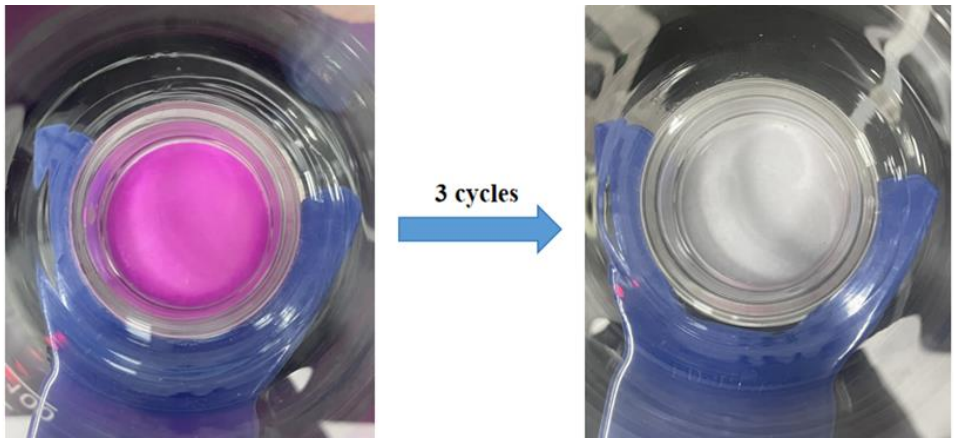

Fig. 10. Comparison of $C_{0.02}$CN/NFC (5%) composite membranes before and after three cycles of self-cleaning test

CONCLUSIONS

1. Carbon-doped g-C_3N_4 material was successfully synthesized by a simple high-temperature process. UV-Vis diffuse results show that the carbon-doped sample

had a smaller bandgap, corresponding to longer wavelengths. This effectively reduced photogenerated carrier recombination and improved photocatalytic ability compared with pure g-C_3N_4. The more the carbon doping, the longer the wavelength of light absorbance.

2. Composite membranes were prepared using a simple vacuum filtration method. Examining the water flux analysis of composite membranes with different nanofibrillated cellulose (NFC) contents and different carbon doping contents, it can be seen that the increase of the proportion of NFC and the increase of carbon doping content increased the water flux of g-C_3N_4/NFC composite membranes, and all the composite membranes exhibited higher water flux than that of the pure g-C_3N_4. When the proportion of NFC was 15%, the $C_{0.02}$CN/NFC composite membrane's water flux reached a maximum value of 75.7 $L \cdot m^{-2} \cdot h^{-1} \cdot bar^{-1}$ under filtration-only conditions.
3. Through exploring the retention and self-cleaning performance of the composite membrane, a large enlargement in flux and retention between the dark and light irradiation conditions was found for the treatment of organic dyes with smaller molecule sizes. The retention efficiency and flux of the composite membrane increased with an increase in the carbon doping content; the retention rate of the composite membrane was 80.8% for the $C_{0.02}$CN/NFC (5%) composite membrane, and the recovery of flux after photocatalytic irradiation reached 92.3%.
4. Moreover, good retention rate and feed flux of the composite membrane in three cycles of photocatalytic experiments confirmed the good self-cleaning ability and long-term stability of the composite membrane. Hence, the designed photocatalytic membranes were judged to have huge potential to be used for wastewater treatment and water purification in the industry. This technique also could be applied to other materials with nanosheet structure.

ACKNOWLEDGMENTS

The authors are grateful for the support of Research Project of Fashu Foundation (Grant No. MFK23007), the Science and Technology Department of Fujian (Grant No. 2023J011394), and Principal Funding of Minjiang University (Grant No. 103952023071).

REFERENCES CITED

Asaithambi, P., Yesuf, M. B., Govindarajan, R., Hariharan, N. M., Thangavelu P., Alemayehu, E. (2022). "A review of hybrid process development based on electrochemical and advanced oxidation processes for the treatment of industrial wastewater," *Inter. J. Chem. Reactor Eng.* 22, article 1105376. DOI: 10.1155/2022/1105376

Cao, L. L., Jiang, S. Q., Ling, Z. Y., Wang, C., Xu, X., Wang, L. (2018). "Properties and mechanisms of tetracycline photocatalytic degradation by hydrothermal synthesis Ag-$SrTiO_3$ in visible-light," *Chem. Indus. Eng. Prog.* 37(11), 4500-4508. DOI: 10.16085/j.issn.1000-6613.2018-0499

Chakravorty, A., and Roy, S. (2024). "A review of photocatalysis, basic principles, processes, and materials," *Sus. Chem. Environ.* 8, article 100155. DOI: 10.1016/j.scenv.2024.100155

Dou, Q., Hou, J. H., Hussain, A., Zhang, G., Zhang, Y., Luo, M., Wang, X., and Cao, C. (2022). "One-pot synthesis of sodium-doped willow-shaped graphitic carbon nitride for improved photocatalytic activity under visible-light irradiation," *J. Colloid Interface Sci.* 624, 79-87. DOI: 10.1016/j.jcis.2022.05.085

Fouda, A., Hassan, S., Saied E., and Hamza, M. (2021). "Photocatalytic degradation of real textile and tannery effluent using biosynthesized magnesium oxide nanoparticles (MgO-NPs), heavy metal adsorption, phytotoxicity, and antimicrobial activity," *J. Environ. Chem. Eng.* 9, article 105346. DOI: 10.1016/j.jece.2021.105346

Hafeez, H. Y., Lakhera, S. K., Shankar, M. V., and Bernaurdshaw, N. (2020). "Synergetic improvement in charge carrier transport and light harvesting over ternary $InVO_4$-g-C_3N_4/rGO hybrid nanocomposite for hydrogen evolution reaction," *Inter. J. Hydro. Energy* 45(13), 7530-7540. DOI: 10.1016/j.ijhydene.2019.05.235

Hou, J. H., Zhang, T. T., Jiang, T., Wu, X., Zhang, Y., Tahir, M., Hussain, A., Luo, M., Zou, J., and Wang, X. (2021). "Fast preparation of oxygen vacancy-rich 2D/2D bismuth oxyhalides-reduced graphene oxide composite with improved visible-light photocatalytic properties by solvent-free grinding," *J. Clean. Prod*. 328, article ID article 129651. DOI: 10.1016/j.jclepro.2021.129651

Huang, L., Liu, J., Li, P., Li, Y., Wang, C., Shu, S., and Song, Y. (2022). "CQDs modulating Z-scheme g-C_3N_4/BiOBr heterostructure for photo-catalytic removing RhB, BPA and TC and *E. coli* by LED light," *J. Alloy Compd*. 895, article ID article 162637. DOI: 10.1016/j.jallcom.2021.162637

Hussain, A., Hou, J. H., Tahir, M., Wang, X., Qadri, M. U., Jiang, T., Tu, X., Zhang, T., Dou, Q., and Zou, J. (2021). "Fine-tuning internal electric field of BiOBr for suppressed charge recombination," *J. Environ. Chem. Eng.* 9(1), article 104766. DOI: 10.1016/j.jece.2020.104766

Hussain, A., Hou, J. H., Wang, X., Hussain, A., Hou, J., Tahir, M., Ali, S. S., Rehman, Z. U., Bilal, M., Zhang, T., *et al.* (2022). "Recent advances in BiOX-based photocatalysts to enhanced efficiency for energy and environment applications," *Catal. Rev*. 66(1), 1-55. DOI: 10.1080/01614940.2022.2041836

Jiang, J., Cao, S. W., Hu, C. L., and Chen, C. H. (2017). "A comparison study of alkali metal-doped g-C_3N_4 for visible-light photocatalytic hydrogen evolution," *Chin. J. Catal*. 38(12), 1981-1989. DOI: 10.1016/S1872-2067(17)62936-X

Kuang, L., Chen, Z., Yan, Y., Guo, F., and Shi, W. (2024). "Research progress of g–C_3N_4–based materials for photothermal-assisted photocatalysis," *Inter. J. Hydrogen Energy* 87(18), 20-49. DOI: 10.1016/j.ijhydene.2024.09.009

Liang, Y., Lin, X., Kong, X., Duan, Q., Wang, P., Mei, X., Ma, J. (2021). "Making waves: Zero liquid discharge for sustainable industrial effluent management," *Water* 13, 1-8. DOI: 10.3390/w13202852

Liu, T. T., Wang, L., Liu, X., Sun, C., Lv, Y., Miao, R., and Wang, X. (2020). "Dynamic photocatalytic membrane coated with $ZnIn_2S_4$ for enhanced photocatalytic performance and antifouling property," *Chem. Eng. J*. 379, article ID 122379. DOI: 10.1016/j.cej.2019.122379

Mohammad, A., Khan M. E., Yoon, T., and Cho, M. H. (2020). "Na, O-co-doped-graphitic-carbon nitride (Na, O-g-C_3N_4) for nonenzymatic electrochemical sensing of

hydrogen peroxide," *Appl. Surf. Sci.* 525, article ID 146353. DOI: 10.1016/j.apsusc.2020.146353

Pan, J., Hua, D., Hong, Y., Cheng, X., Guo, F., Tan, K. B., Zhong, Z., and Zhan, G. (2023). "Design of hybrid g-C_3N_4/GO/MCE photocatalytic membranes with enhanced separation performance under visible-light irradiation," *Chem. Eng. J.* 466, article 143164. DOI: 10.1016/j.cej.2023.143164

Praus, P. (2022). "A brief review of s-triazine graphitic carbon nitride," *Carbon Lett*. 32 (3), 703-712. DOI: 10.1007/s42823-022-00319-9

Rehman, Z. U., Bilal, M., Hou, J. H., Butt, F., Ahmad, J., Ali, S. A. M., and Hussain, A. (2022). "Photocatalytic CO_2 reduction using TiO_2-based photocatalysts and TiO_2 Z-scheme heterojunction composites: A review," *Molecules* 27(7), article 2069. DOI: 10.3390/molecules27072069

Samuel, S. E., Ibrahim, L., Zhou, W., Jiang, Y., Zhang, Q., Xiao, W., Zhang, M., Fernando, G. F., and Yuan, Z. (2020). "Synthesis and characterization of triazole based sulfonated nanocrystalline cellulose proton conductor," *Cellulose* 27(6), 3197-3209. DOI: 10.1007/s10570-020-02981-6

Sahoo, R. C., Lu, H., Garg, D., Yin, Z., and Matte, R. (2022). "Bandgap engineered g-C_3N_4 and its graphene composites for stable photoreduction of CO_2 to methanol," *Carbon* 192, 101-108. DOI: 10.1016/j.carbon.2022.02.021

Seddiqi, H., Oliaei, E., Honarkar, H., Jin, J., Geonzon, L.C., Bacabac, R. G., Jenneke K.-N. (2021), "Cellulose and its derivatives: towards biomedical applications" *Cellulose* 28, 1893-1931. DOI: 10.1007/s10570-020-03674-w

Shen, L., Shi, Q., Zhang, S., Gao, J., Cheng, D. C., Yi, M., Song, R. Wang, L., Jiang, J., Karnik, R., and Zhang, S. (2021). "Highly porous nanofiber-supported monolayer graphene membranes for ultrafast organic solvent nanofiltration," *Sci. Adv.* 7, article eabg6263. DOI: 10.1126/sciadv.abg6263

Shibu, A., Dsouza, A., Akkera, H. S., Giresha, A. S., and Kambhala, N. (2024). "Structural, optical, and photocatalytic properties of nano-scaled g-C_3N_4 materials," *Appl. Phys. A* 130, article 431. DOI: 10.1007/s00339-024-07563-y

Wang, C., Lu, Y., Wang, Z., Liao, H., Zhou, W., He, Y., Osman, S. M., An, M., Asakura, Y., Yamauchi, Y., *et al.* (2024). "Salt-assisted construction of hydrophilic carbon nitride photocatalyst with abundant water molecular adsorption sites for efficient hydrogen production," *Appl. Catal. B-Environ.* 350, article ID 123902. DOI: 10.1016/j.apcatb.2024.123902

Wang, F., Xu, J., Wang, Z., Lou, Y., Pan C., and Zhu Y. (2022). "Unprecedentedly efficient mineralization performance of photocatalysis-self-Fenton system towards organic pollutants over oxygen-doped porous g-C_3N_4 nanosheets," *Appl. Catal. B-Environ.* 312, article ID 121438. DOI: 10.1016/j.apcatb.2022.121438

Wang, X., Ren, Y., Li, Y., and Zhang, G. (2022). "Fabrication of 1D/2D $BiPO_4$/g-C_3N_4 heterostructured photocatalyst with enhanced photocatalytic efficiency for NO removal," *Chemosphere* 287(2), article ID 132098. DOI: 10.1016/j.chemosphere.2021.132098

Wang, Y., Liu, L., Ma, T., Zhang, Y., and Huang, H. (2021). "2D graphitic carbon nitride for energy conversion and storage," *Adv. Funct. Mater.* 31(34), article 102540. DOI: 10.1002/adfm.202102540

Wen, J., Xie, J., Chen, X., and Li, X. (2017). "A review on g-C_3N_4-based photocatalysts," *Appl. Surf. Sci*. 391, 72-123. DOI: 10.1016/j.apsusc.2016.07.030

Wu, M., He, X., Jing, B., Wang, T., Wang, C., Qin, Y., Ao, Z., Wang, S., and An, T. (2022). "Novel carbon and defects co-modified g-C_3N_4 for highly efficient photocatalytic degradation of bisphenol A under visible light," *J. Hazard. Mater*. 384, article ID 121323. DOI: 10.1016/j.jhazmat.2019.121323

Yang, Z. M., Lin, Q. Q., Zeng, G. Y., Zhao, S. M., Yan, G. L., Ang, M. B. M. Y., Chiao, Y. H., and Pu, S. Y. (2023). "Ternary hetero-structured BiOBr/Bi_2MoO_6@MXene composite membrane: Construction and enhanced removal of antibiotics and dyes from water," *J. Membr. Sci*. 669, article ID 121329. DOI: 10.1016/j.memsci.2022.121329

Zhu, Y., Wang, T., Xu, T., Li, Y., and Wang, C. (2019). "Size effect of Pt co-catalyst on photocatalytic efficiency of g-C_3N_4 for hydrogen evolution," *Appl. Surf. Sci.* 464, 36-42. DOI: 10.1016/j.apsusc.2018.09.061

Zhang, T. T., Chen, L. F., Jiang, T., Hou, J. H., Zhang, G., and Hussain, A. (2021). "Chemical precipitation synthesis of $Bi_{0.7}Fe_{0.3}OCl$ nanosheets via Fe (III)-doped BiOCl for highly visible light photocatalytic performance," *Mater. Today Commun.* 26, article ID 102145. DOI: 10.1016/j.mtcomm.2021.102145

Zhou, W., Sun, S., Jiang, Y., Zhang, M., Lawan, I., Fernando, G. F., Wang, L., Yuan, Z. (2019). "Template in situ synthesis of flower-like BiOBr/microcrystalline cellulose composites with highly visible light photocatalytic activity," *Cellulose* 26, 9529-9541. DOI: 10.1007/s10570-019-02722-4

Zhou, W., Huang, H., Wu, Y., Wang, J., Yamauchi, Y., Kim, J., Osman S. M., Xu, X., Wang, L., Wang. C., Yuan, Z. (2023). "Construction of a 2D lamellar membrane for a combination of photocatalytic hydrogen evolution and photothermal water evaporation," *Chem. Eng. J.* 471, article 144395. DOI: g/10.1016/j.cej.2023.144395

Zhu, J. N., Zhu, X.Q., Cheng, F. F., Li, P., Wang, F., Xiao, Y. W., Xiong, W. W. (2019). "Preparing copper doped carbon nitride from melamine templated crystalline copper chloride for Fenton-like catalysis," *Appl. Catal. B* 256, article 117830. DOI: 10.1016/j.apcatb.2019.117830.

Article submitted: September 20, 2024; Peer review completed: November 2, 2024; Revised version received: November 12, 2024; Accepted: November 15, 2024; Published: November 25, 2024.
DOI: 10.15376/biores.20.1.809-825